The EMBO Journal (2007) 26, 4433–4444 | © 2007 European Molecular Biology Organization | Some Rights Reserved 0261-4189/07
www.embojournal.org

THE EMBO JOURNAL

EMBO open

Coupling of protein localization and cell movements by a dynamically localized response regulator in *Myxococcus xanthus*

Simone Leonardy[1], Gerald Freymark[1], Sabrina Hebener[1], Eva Ellehauge[2] and Lotte Søgaard-Andersen[1,*]

[1]Department of Ecophysiology, Max Planck Institute for Terrestrial Microbiology, Marburg, Germany and [2]Department of Biochemistry and Molecular Biology, University of Southern Denmark, Odense M, Denmark

Myxococcus xanthus **cells harbor two motility machineries, type IV pili (Tfp) and the A-engine. During reversals, the two machineries switch polarity synchronously. We present a mechanism that synchronizes this polarity switching. We identify the *r*equired f*o*r *m*otility *r*esponse regulator (RomR) as essential for A-motility. RomR localizes in a bipolar, asymmetric pattern with a large cluster at the lagging cell pole. The large RomR cluster relocates to the new lagging pole in parallel with cell reversals. Dynamic RomR localization is essential for cell reversals, suggesting that RomR relocalization induces the polarity switching of the A-engine. The analysis of RomR mutants shows that the output domain targets RomR to the poles and the receiver domain is essential for dynamic localization. The small GTPase MglA establishes correct RomR polarity, and the Frz two-component system regulates dynamic RomR localization. FrzS localizes with Tfp at the leading pole and relocates in an Frz-dependent manner to the opposite pole during reversals; FrzS and RomR localize and oscillate independently. The Frz system synchronizes these oscillations and thus the synchronous polarity switching of the motility machineries.**

The EMBO Journal (2007) **26,** 4433–4444. doi:10.1038/sj.emboj.7601877; Published online 11 October 2007
Subject Categories: cell & tissue architecture; microbiology & pathogens
Keywords: A-motility; morphogenetic cell movements; *Myxococcus xanthus*; polarity; response regulator

Introduction

The formation of spatial patterns of cells is a recurring theme in developmental biology. The mechanisms underlying these pattern formation processes often include directed, morphogenetic cell movements. An example is provided by cells of the bacterium *Myxococcus xanthus*, which display two types of morphogenetic cell movements depending on their nutritional status, and which result in the formation of two distinct structures, colonies and fruiting bodies (Søgaard-Andersen, 2004). In the presence of nutrients, colonies form, and the cells at the edge spread coordinately outward. In the absence of nutrients, the spreading behavior is constrained and cells aggregate to construct multicellular fruiting bodies. The cells in the fruiting bodies differentiate into spores. The formation of these two spatial cell patterns depends on the ability of the cells to actively move and to regulate their motility behavior.

The rod-shaped *M. xanthus* cells move by gliding in the direction of their long axis, and active movements are restricted to solid surfaces. Two distinct motility systems are involved: the social (S)- and the adventurous (A)-motility systems (Hodgkin and Kaiser, 1979). Generally, mutations only affect one of the two systems; however, mutations in *mglA*, which encodes a member of the Ras superfamily of small GTPases (Hartzell, 1997), abolish the activity of both systems (Hodgkin and Kaiser, 1979).

The S-motility system depends on type IV pili (Tfp) and is the equivalent of twitching motility in *Neisseria* and *Pseudomonas* species (Mattick, 2002). In *M. xanthus*, this Tfp motility is dependent on cell–cell contact and is active when cells are within contact distance of each other (Hodgkin and Kaiser, 1979). Tfp localize to the leading cell pole (Mignot *et al*, 2005), and a motive force is generated by retraction of Tfp (Merz *et al*, 2000; Sun *et al*, 2000; Skerker and Berg, 2001).

The A-motility system provides cells with the ability to move as single cells. It is currently unknown how motive force is generated in the A-motility system. However, two models have been suggested for force generation in this motility system. In one model, the A-motility system functions similarly to junctional pore complexes in gliding cyanobacteria, which generate force by polyelectrolyte secretion (Hoiczyk and Baumeister, 1998; Wolgemuth *et al*, 2002). In *M. xanthus*, structures equivalent to the junctional pore complexes, called A-motility nozzles, are present at both poles, and force generation has been suggested to involve polyelectrolyte secretion from nozzles at the lagging pole (Wolgemuth *et al*, 2002). An A-motility model involving polymer export is supported by the requirement of a large number of genes for A-motility that encode proteins involved in polymer synthesis and export (Youderian *et al*, 2003; Yu and Kaiser, 2007). In an alternative model, force generation involves multiple adhesion complexes assembled at the leading cell pole and distributed along the cell body (Mignot *et al*, 2007). These complexes are defined by the

*Corresponding author. Department of Ecophysiology, Max Planck Institute for Terrestrial Microbiology, Karl-von-Frisch Strasse, Marburg 35043, Germany. Tel.: +49 6421 178201; Fax +49 6421 178209; E-mail: sogaard@mpi-marburg.mpg.de

Received: 29 July 2007; accepted: 11 September 2007; published online: 11 October 2007

AglZ protein and are thought to function in a manner similar to that of focal adhesion complexes in eukaryotic cells (Mignot *et al*, 2007).

As *M. xanthus* cells move over a surface, they periodically stop and then resume gliding in the opposite direction, with the old lagging pole becoming the new leading pole (Blackhart and Zusman, 1985). Regulation of the cell reversal frequency is critical for establishing both types of morphogenetic cell movements (Blackhart and Zusman, 1985). The reversal frequency is regulated by the Frz two-component system (Blackhart and Zusman, 1985). Analysis of single-cell behavior as well as colony expansion rates suggests that the A- and S-motility systems generate motive force in the same direction (Kaiser and Crosby, 1983; Spormann, 1999) and that the directionality of the two engines changes synchronously during reversals (Kaiser and Crosby, 1983; Blackhart and Zusman, 1985). The mechanism underlying a direction change in the S-motility system involves an Frz-dependent switch of the pole, at which Tfp assemble and with the FrzS protein relocating from the old leading to the new leading cell pole (Mignot *et al*, 2005). In the A-motility system, the change in directionality involves the Frz-dependent relocation of the AglZ protein from the old leading cell pole to the new leading cell pole (Mignot *et al*, 2007).

To further the understanding of the A-motility system and the mechanisms underlying polarity switching, we focused on the *r*equired f*o*r *m*otility *r*esponse regulator (RomR). We identify RomR as essential for A-motility. RomR localizes in a bipolar, asymmetric pattern with a large cluster at the lagging pole. In synchrony with cell reversals, the large RomR cluster relocates in an Frz-dependent manner to the new lagging pole. Our data suggest that the large RomR cluster stimulates the A-motility machinery at the lagging pole and that dynamic RomR localization is essential for polarity switching of the A-motility system. Moreover, we show directly that RomR and FrzS oscillate between the cell poles independently but synchronously, thus ensuring the synchronous polarity switching of the two motility systems.

Results

RomR is required for A-motility

While analyzing the ORF *MXAN4462*, which is required for fruiting body formation in *M. xanthus* (Freymark *et al*, unpublished), we also analyzed the downstream ORF, *MXAN4461*. The deduced MXAN4461 protein encodes an uncharacterized response regulator, RomR (Figure 1A). RomR consists of an N-terminal receiver domain of two-component systems (residues 1–116) and a C-terminal output domain (residues 117–420) that can be subdivided into a Pro-rich region (residues 117–368) and a Glu-rich tail (residues 369–420) (Figure 1C–E). Database searches revealed that several bacteria belong to the δ-proteobacteria, which like *M. xanthus*, encode a protein with a domain structure similar to that of RomR (Supplementary Table I). The function of these response regulators is unknown. To understand the function of RomR in *M. xanthus*, we created an insertion mutation in which an *nptII* gene was inserted at codon 30 in *romR* (*romR*::*nptII*) in the fully motile strain DK1622, which serves as the wild-type strain in this work. The resulting strain, SA1128, was analyzed further.

Strain SA1128 (*romR*::*nptII*) was indistinguishable from the wild type with respect to growth in rich medium and in chemically defined A1 minimal medium (data not shown). We tested whether SA1128 was deficient in motility by examining colony spreading on 1.5% agar, which favors motility by means of the A-motility system (Shi and Zusman, 1993). Under these conditions, the wild-type strain formed large colonies with rafts of cells and single cells at the edge. Strain SA1128 formed small colonies, and rafts of cells but no single cells were observed at the edge (Figure 2A). When analyzed on 0.5% agar, which favors motility by means of the S-motility system, SA1128 formed colonies that were only slightly smaller than those of wild-type cells (data not shown). These observations suggested that the *romR* mutation caused an A-motility defect. We investigated this hypothesis by introducing the *romR* mutation into strains containing mutations that inactivated either the A-motility system (A^-S^+) or the S-motility system (A^+S^-). The *romR* mutation did not interfere with S-motility in the A^-S^+ strain, but it abolished A-motility in the A^+S^- strain (Supplementary Figure 1). To conclusively determine whether *romR* is required for A-motility, we analyzed movement of single cells on 1.5% agar by time-lapse microscopy. In these recordings, SA1128 did not display any single-cell movement, whereas wild-type cells displayed normal single-cell movements (data not shown). Thus, the *romR* mutation results in an A-motility defect.

To determine whether the *romR* mutation caused a defect in fruiting body formation, cells were exposed to starvation. Wild-type cells had completed fruiting body formation at 72 h, whereas SA1128 cells formed many small, abnormally shaped fruiting bodies (Figure 2B). Moreover, the sporulation frequency of SA1128 was only 3% that of wild-type cells.

We then integrated a $romR^+$ allele including the native promoter by site-specific recombination at the chromosomal Mx8 attachment site in SA1128, yielding strain SA2272. In this complementation experiment, the $romR^+$ allele corrected the A-motility defect as well as the developmental defects caused by the *romR* mutation (Figure 2A and B). In contrast, the integrated vector pSWU30 alone (strain SA2210) did not correct these defects (Figure 2A and not shown). Immunoblot analysis using polyclonal rabbit antibodies against full-length RomR confirmed that RomR accumulated at similar levels in SA2272 and wild type (Figure 2C). Taken together, these observations show that RomR is required for A-motility. We speculate that the defect in fruiting body formation results from the defect in the A-motility system.

RomR localizes in a bipolar, asymmetric pattern

Given that RomR plays a role in A-motility, we hypothesized that RomR might function in a spatially confined manner. To test this idea, we used the green fluorescent protein (GFP) as a fluorescent marker in localization studies. A *romR-gfp* allele including the native *romR* promoter was integrated at the chromosomal Mx8 attachment site in the wild type and in strain SA1128 (*romR*::*nptII*), giving rise to strains SA2273 and SA2271, respectively. RomR-GFP corrected the A-motility defect caused by the *romR* mutation in strain SA2271 (*romR*::*nptII*, *romR-gfp*) (Figure 2A) and did not interfere with the activity of wild-type RomR in strain SA2273 ($romR^+$, *romR-gfp*) (data not shown). Moreover, single cells of SA2271 cells moved with the same speed (3.4 ± 0.2 μm/

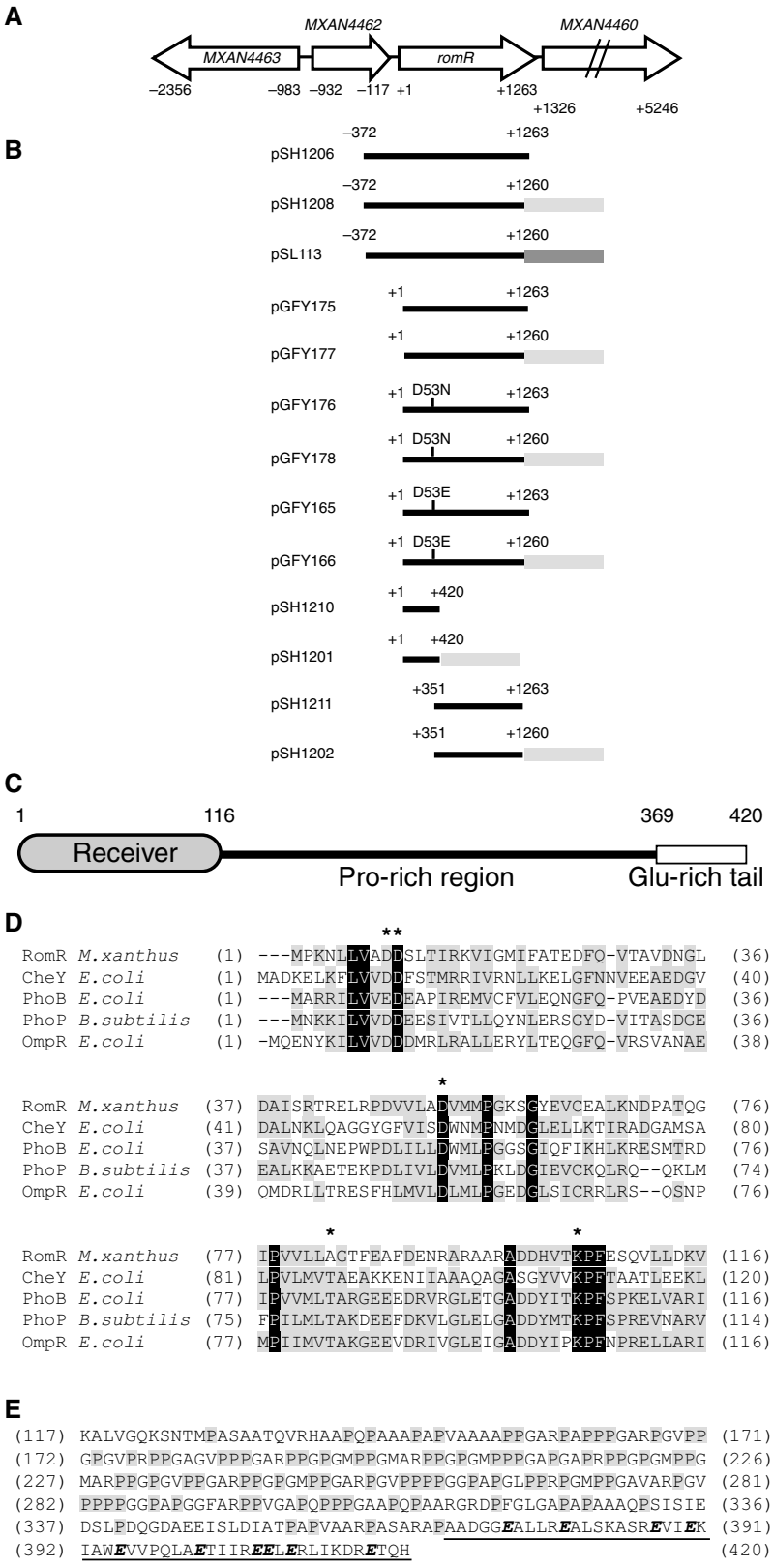

Figure 1 The *romR* locus and the RomR protein. (**A**) Organization of the *romR* locus. Arrows indicate the direction of transcription of *romR* and the flanking ORFs. Coordinates are relative to the start codon of *romR*. The deduced proteins encoded by the flanking ORFs have the following characteristics: MXAN4460 is similar to Val-tRNA synthethases; MXAN4462 contains two CheW domains; MXAN4463 is a response regulator with a GGDEF output domain. (**B**) Plasmids used in this work. Coordinates are relative to the *romR* start codon. Light gray boxes indicate *gfp* and the dark gray box indicates *mDsRed*. (**C**) Scheme of RomR domain structure. (**D**) Alignment of N-terminal receiver domain of RomR with characterized receiver domains. Asterisks indicate conserved signature residues of receiver domains (Stock *et al*, 2000). Residues shaded black are 100% identical, and those shaded gray are 60–100% conserved. (**E**) Primary sequence of RomR output domain. Pro residues in the Pro-rich region are shaded gray. The Glu-rich region is underlined, and Glu residues are in bold and italic.

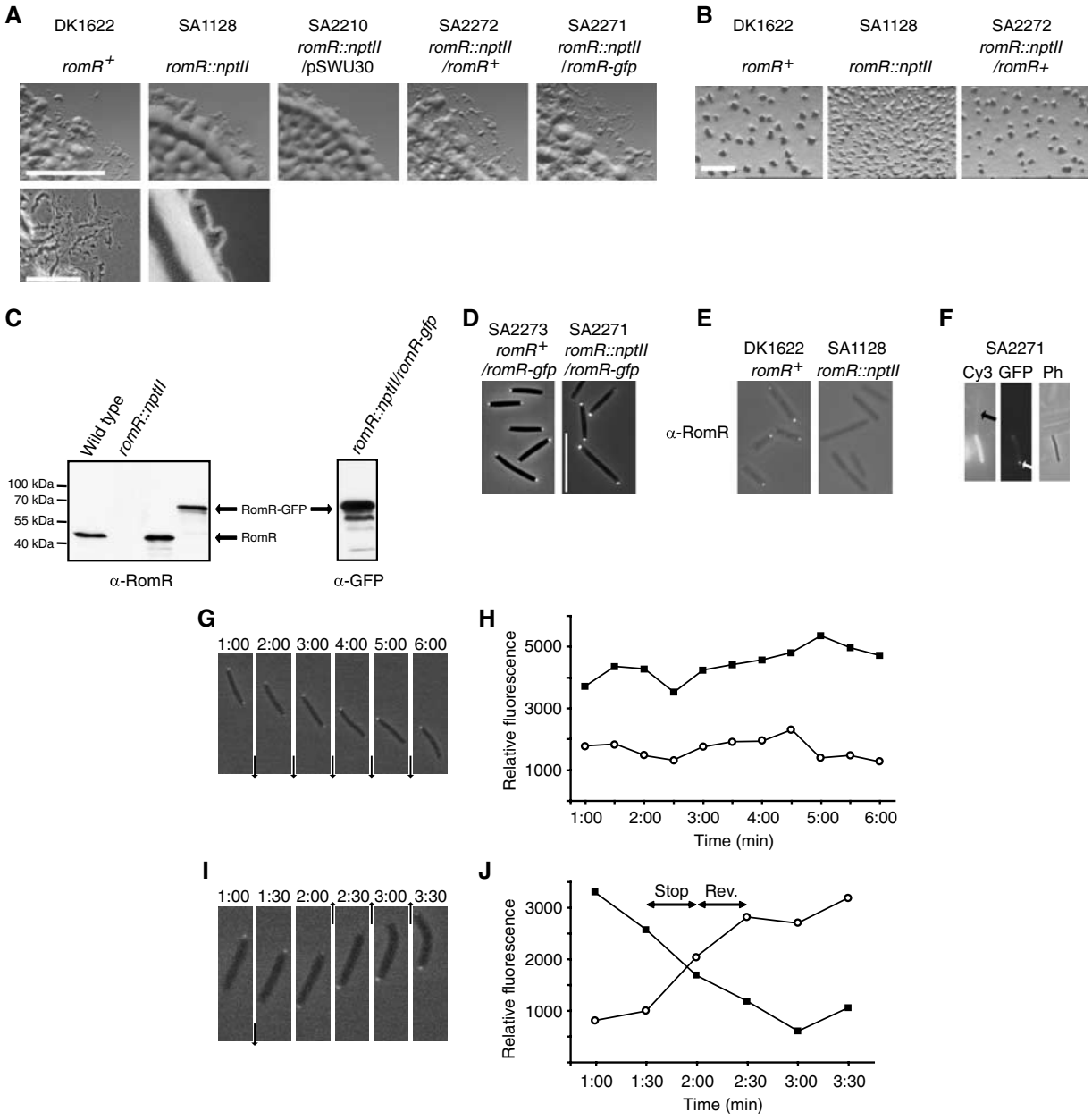

Figure 2 RomR is required for A-motility and localizes in a bipolar, asymmetric pattern. (**A**) Motility phenotype of *romR* mutant. Cells were incubated at 32°C for 24 h on 1.5% agar supplemented with 0.5% CTT medium and visualized with a Leica MZ8 stereomicroscope (upper row) and a Leica IMB/E inverted microscope (lower row). Scale bars: upper row, 5 mm; lower row, 50 μm. (**B**) Developmental phenotype of *romR* mutant. Cells were starved on CF agar for 72 h and visualized with a Leica MZ8 stereomicroscope. Scale bar: 50 μm. (**C**) RomR and RomR-GFP accumulation. Cells from steady-state cultures were harvested, and total protein was separated by SDS–PAGE (1 μg of protein per lane) and analyzed by immunoblotting. Strains used (left to right): DK1622, SA1128, SA2272, and SA2271. The blot on the left was probed with rabbit anti-RomR antibodies and the blot on the right with monoclonal anti-GFP antibodies. RomR and Rom-GFP proteins are indicated. Migration of molecular size markers is indicated on the left. (**D**) Localization of RomR-GFP. Cells were transferred from a steady-state culture to a thin agar pad on a microscope slide and imaged by fluorescence and phase-contrast microscopy. Depicted are overlays of fluorescence and phase-contrast images. Scale bar: 10 μm. (**E**) Localization of RomR by immunofluorescence microscopy. Cells were harvested from 1.5% agar supplemented with 1% CTT, fixed, reacted with affinity-purified anti-RomR antibodies, and imaged by fluorescence and phase-contrast microscopy. Depicted are overlays of fluorescence and phase-contrast images. (**F**) The large RomR-GFP cluster localizes to the pole opposite to that containing Tfp. SA2271 cells were grown as in (E), stained with Cy3, and inspected by fluorescence microscopy to visualize Tfp (Cy3, arrow points to Tfp) and RomR-GFP (GFP, arrow points to large RomR-GFP cluster) and by phase-contrast microscopy (Ph). (**G**) The large RomR-GFP cluster localizes to the lagging pole. Cells of SA2271 were grown as in (D), transferred to a thin agar pad on a microscope slide, and imaged by fluorescence and phase-contrast microscopy at 30-s intervals. Shown is a representative cell that did not reverse. Depicted are overlays of fluorescence and phase-contrast images recorded at the indicated time points in minutes. Arrows indicate the direction of movement. (**H**) Quantitative analysis of polar fluorescence signals. Relative fluorescence intensities (arbitrary units) of each pole in the cell in (D) were measured and plotted as a function of time. Filled squares, lagging pole; open circles, leading pole. (**I**) RomR localization is dynamic. Cells of SA2271 were grown and visualized as in (G). Shown is a representative cell that underwent one reversal. Depicted are overlays of fluorescence and phase-contrast images recorded at the indicated time points in minutes. Arrows indicate the direction of movement. From 1:30 to 2:00, the cell did not move. From 2:00 to 2:30, the cell reversed. (**J**) Quantitative analysis of polar fluorescence signals. Relative fluorescence intensities (arbitrary units) of each pole in the cell in (I) were measured and plotted as a function of time. Filled squares, initial lagging pole; open circles, initial leading pole. Time intervals with a stop or reversal (Rev.) are indicated by double-headed arrows.

min) as single cells of wild type (3.3 ± 0.9 μm/min). These results provided evidence that the fusion protein is fully functional. Immunoblot analysis using antibodies against RomR and GFP confirmed that RomR-GFP (calculated molecular mass 71.3 kDa) accumulated at a level similar to that of RomR in wild-type cells and that degradation was negligible (Figure 2C). Fluorescence microscopy showed that RomR-GFP localized to the cell poles in both SA2271 (*romR*::*nptII*, *romR-gfp*) and SA2273 (*romR*$^+$, *romR-gfp*) (Figure 2D). In both strains, 90% of the cells ($N = 200$) had an asymmetric RomR-GFP distribution, with a large and a small polar cluster; the remaining 10% displayed a bipolar, symmetric localization pattern. To verify the asymmetric distribution, we determined the localization of native RomR in the wild type by immunofluorescence microscopy using affinity-purified RomR antibodies. A bipolar, asymmetric RomR localization pattern was observed; as expected, RomR was not detected in mutant SA1128 (*romR*::*nptII*) (Figure 2E).

The large RomR cluster localizes to the lagging cell pole

To clarify whether the large RomR cluster localized to the leading or lagging cell pole, two different approaches were used. First, RomR-GFP localization was determined relative to Tfp, which are localized to the leading cell pole. In 88% of the cells ($N = 32$) of SA2271 (*romR::nptII*, *romR-gfp*) stained with the fluorescent dye Cy3, the large RomR-GFP cluster was localized to the pole opposite to that containing Tfp, that is, the lagging cell pole (Figure 2F). Second, in time-lapse fluorescence microscopy of SA2271 (*romR::nptII*, *romR-gfp*) and SA2273 (*romR*$^+$, *romR-gfp*) cells moving on a thin agar pad, the bright RomR-GFP cluster was always detected at the lagging cell pole (Figure 2G and H; Table I). In these time-lapse recordings, only cells separated from other cells by at least one cell length were scored to ensure that cells moved only by means of the A-motility system. We observed the same RomR-GFP localization pattern in a Δ*pilA*, *romR::nptII* mutant (SA2289), which lacks Tfp-dependent motility owing to an in-frame deletion of the *pilA* gene, which encodes the Tfp subunit (Table I). Thus, in cells moving by means of the A-motility system, the large RomR cluster is at the lagging pole.

RomR localization is dynamic

To resolve whether RomR localization changes during a reversal, RomR-GFP location was analyzed during reversals in single cells of SA2271 (*romR::nptII*, *romR-gfp*). Thirty-two reversals were observed, and all reversals were accompanied by a switch in localization of the large RomR-GFP cluster from the old lagging pole to the new lagging pole (Figure 2I; Table I). Quantification of the fluorescence intensity of the RomR-GFP clusters during reversals revealed the following order of events (data for a representative cell are shown in Figure 2J). Initially, the fluorescence intensity of the cluster at the lagging pole was greater than that of the cluster at the leading pole, and the cell moved in one direction. The fluorescence intensity of the two polar clusters then became similar, as the intensity of the cluster at the lagging pole decreased and the intensity of the cluster at the leading pole increased. At the same time, the cell stopped moving. As the intensity of the cluster at the old lagging pole continued to decrease and the intensity of the cluster at the old leading pole continued to increase, the cell began to move in the opposite direction. Similar observations were made in single cells of the mutant SA2289 (Δ*pilA*, *romR*::*nptII*, *romR-gfp*), which harbors only an active A-motility system (data not shown; Table I).

To determine the mechanism underlying dynamic RomR localization, we followed RomR-GFP in single cells of strain SA2271 (*romR*::*nptII*, *romR-gfp*). Cells treated with 25 μg/ml chloramphenicol to inhibit protein synthesis displayed a

Table I Quantitative analysis of the localization of RomR-GFP proteins

Strain	Strain background	GFP construct[a]	% cells with large RomR cluster at lagging pole/leading pole/symmetric clusters[b]	Cellular reversals	RomR relocation during reversal
SA2273	*romR*$^+$	P_{nat}-RomR-GFP	100/0/0	ND	ND
SA2271	*romR*::*nptII*	P_{nat}-RomR-GFP	100/0/0	32	32
SA2289	Δ*pilA*, *romR*::*nptII*	P_{nat}-RomR-GFP	97/3/0	20	20
SA2058	*romR*::*nptII*	P_{pilA}-RomR-GFP	100/0/0	30	30
SA2259	*romR*::*nptII*	P_{pilA}-receiver-GFP	Homogeneous distribution[c]	NA[c]	NA[c]
SA2260	*romR*::*nptII*	P_{pilA}-output-GFP	88/12/0	3	0
SA2062	*romR*::*nptII*	P_{pilA}-RomR^{D53N}-GFP	100/0/0	0	0
SA2060	*romR*::*nptII*	P_{pilA}-RomR^{D53E}-GFP	100/0/0	45	45
SA2070	*frzE*::Tn*5*(Tet^r)Ω231, *romR*::*nptII*	P_{pilA}-RomR-GFP	100/0/0	0	0
SA2068	*frzE*::Tn*5*(Tet^r)Ω231, *romR*::*nptII*	P_{pilA}-RomR^{D53N}-GFP	100/0/0	0	0
SA2054	*frzE*::Tn*5*(Tet^r)Ω231, *romR*::*nptII*	P_{pilA}-RomR^{D53E}-GFP	71/0/29	43	29[d]
SA2042	*mglA9*	P_{nat}-RomR-GFP	10 bipolar asymmetric/90 unipolar[c]	NA[c]	NA[c]
SA2268	Δ*frzS*	P_{nat}-RomR-GFP	100/0/0	34	34

NA, not applicable; ND, not determined.
[a]In P_{nat} and P_{pilA} constructs, the *gfp* fusion alleles were transcribed from the native *romR* promoter and the *pilA* promoter, respectively.
[b]For each strain, 50 cells were followed for 10 min in time-lapse fluorescence microscopy. Cells were imaged at 30-s intervals. Cells were observed on agar pads covered with a coverslip. All cells scored were separated from other cells by at least one cell length to ensure that cells moved only by means of the A-motility system.
[c]Cells of SA2259 and SA2042 did not move as single cells.
[d]These 29 reversals were all observed in cells with bipolar, asymmetric RomR-GFP localization. The remaining 14 reversals occurred in cells with bipolar, symmetric RomR-GFP localization.

motility pattern and a RomR-GFP localization pattern similar to that of untreated cells (data not shown). This suggests that the mechanism underlying dynamic RomR localization involves the transfer of RomR between the poles and not proteolysis at the old lagging pole accompanied by localization of *de novo*-synthesized protein at the new lagging pole.

Targeting determinants in RomR

To test whether the two domains in RomR have specific functions in RomR localization, genes encoding full-length RomR, the receiver domain plus 24 additional amino acids (residues 1–140 of RomR), and the output domain (residues 117–420 of RomR) were each expressed separately from the *pilA* promoter in the *romR* mutant. The genes encoding these three proteins fused to GFP (RomR-GFP, receiver-GFP, and output-GFP) were also expressed from the *pilA* promoter in the *romR* mutant. In immunoblots, neither the receiver (calculated molecular mass 15.1 kDa) nor the receiver-GFP (calculated molecular mass 42.2 kDa) was detected by anti-RomR antibodies. As the receiver-GFP protein was detected by anti-GFP antibodies (Figure 3C), the receiver-GFP protein was stably synthesized and the anti-RomR antibodies did not recognize the receiver domain. In the strain encoding the output domain, a larger protein (39 kDa) than expected (29.3 kDa) was detected by the anti-RomR antibodies. We attribute this difference to an abnormal mobility of the output

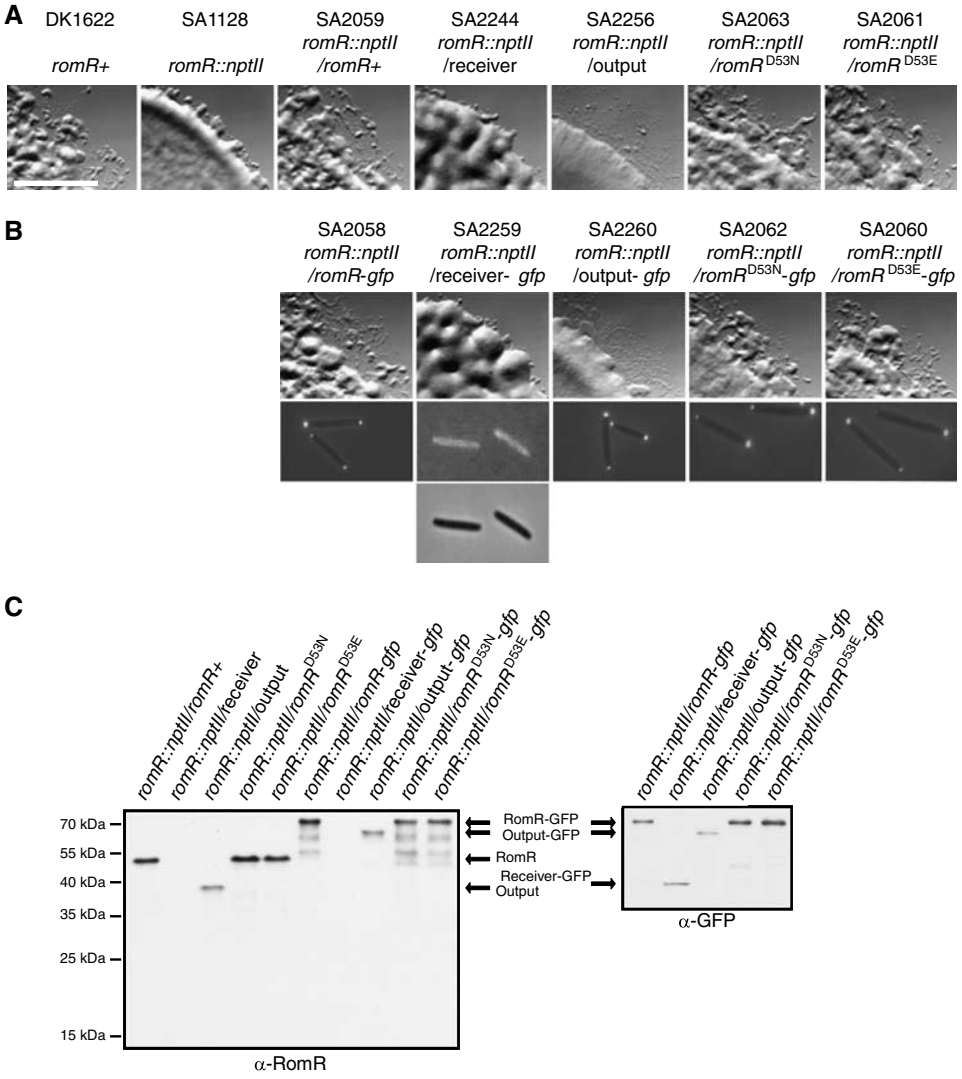

Figure 3 The RomR output domain is sufficient for bipolar, asymmetric localization. (**A**) Motility phenotype of *romR* mutant complemented with different *romR* alleles. Cells were incubated at 32°C for 24 h on 0.5% CTT medium/1.5% agar and visualized with a Leica MZ8 stereomicroscope. Scale bar: 5 mm. (**B**) Motility phenotype of *romR* mutant complemented with different *romR-gfp* alleles and localization of the corresponding GFP fusion proteins. For the experiments shown in the upper row, cells were incubated and visualized as in (A). For the experiments shown in the lower rows, cells were transferred from a steady-state culture to an agar pad on a slide and imaged by fluorescence and phase-contrast microscopy. Depicted are overlays of fluorescence and phase-contrast images, except for the strain containing the receiver-GFP construct for which the images are shown separately. (**C**) Immunoblots of accumulated mutant RomR and RomR-GFP proteins. Cells were grown as in (B) and harvested, and total protein (1 μg per lane) was separated by SDS–PAGE and analyzed by immunoblotting. Strains used in the left blot (left to right): SA2059, SA2244, SA2256, SA2063, SA2061, SA2058, SA2259, SA2260, SA2062, and SA2060. Strains used in the right blot (left to right): SA2058, SA2259, SA2260, SA2062, and SA2060. The left blot was probed with rabbit anti-RomR antibodies, and the right blot was probed with monoclonal anti-GFP antibodies. The different RomR and RomR-GFP proteins are indicated. The migration of molecular size markers is indicated on the left.

domain in the SDS–polyacrylamide gel owing to the unusual sequence of the domain. The output-GFP protein with the expected size (calculated molecular mass 56.4 kDa) was detected by both the anti-RomR and anti-GFP antibodies. Both output domain proteins accumulated at slightly lower levels than full-length RomR (Figure 3C).

Full-length RomR (SA2059) as well as RomR-GFP (SA2058) restored the ability of *romR* mutant cells to move as single cells and, thus, corrected the A-motility defect in the *romR* mutant (Figure 3A and B; Table I). However, neither the receiver domain (SA2244) nor the receiver-GFP protein (SA2259) corrected the A-motility defect in the *romR* mutant (Figure 3A and B; Table I). Moreover, the receiver-GFP protein was homogeneously distributed throughout the cells and failed to segregate to the poles (Figure 3B; Table I). The output domain (SA2256) as well as the output-GFP protein (SA2260) restored the ability of *romR* mutant cells to move as single cells (Figure 3A and B; Table I). The output-GFP protein localized in a bipolar, asymmetric pattern, with 88% of the cells having a large cluster at the lagging pole and 12% having a large cluster at the leading pole (Table I). Cells only rarely reversed, and these rare reversals were not accompanied by a switch in the localization of the output-GFP protein (Table I). These results suggest that the output domain is a pole-targeting determinant, that the receiver domain is involved in dynamic RomR localization, and that dynamic RomR localization is required for reversals.

For many response regulators, it has been shown that phosphorylation of a conserved Asp residue in the receiver domain is required for activity (Stock *et al*, 2000). To test genetically whether phosphorylation of RomR contributes to RomR function and localization, genes encoding two RomR mutant proteins in which the phosphorylatable Asp (D53) in the receiver domain had been substituted were expressed from the *pilA* promoter in the *romR* mutant. In $RomR^{D53N}$, D53 was substituted with Asn, resulting in loss of the ability to be phosphorylated. In $RomR^{D53E}$, D53 was substituted with Glu; in several response regulators, this substitution partially mimics the phosphorylated state (Domian *et al*, 1997). The genes encoding $RomR^{D53N}$ and $RomR^{D53E}$ fused to GFP were also expressed from the *pilA* promoter in the *romR* mutant. Immunoblots with anti-RomR and anti-GFP antibodies confirmed that all four proteins accumulated at levels similar to that of RomR, when wild-type *romR* was expressed from the *pilA* promoter (Figure 3C). All four mutant proteins restored the ability of *romR* mutant cells to move as single cells (Figure 3A and B; Table I). $RomR^{D53N}$-GFP (SA2062) localized in a bipolar, asymmetric pattern, with the large cluster at the lagging pole in all cells observed (Figure 3B; Table I). In contrast to cells synthesizing RomR-GFP, cells synthesizing $RomR^{D53N}$-GFP did not reverse direction, and $RomR^{D53N}$-GFP did not relocate between poles (Table I). $RomR^{D53E}$-GFP (SA2060) also localized in a bipolar, asymmetric pattern, with the large cluster at the lagging pole in all cells observed (Figure 3B; Table I). But these cells displayed a 1.5-fold higher reversal frequency than cells synthesizing RomR-GFP (cf. SA2058 in Table I), and all reversals were accompanied by relocation of the large RomR cluster from the old to the new lagging pole (Table I). The opposite reversal phenotypes of $RomR^{D53N}$-GFP and $RomR^{D53E}$-GFP suggested that $RomR^{D53E}$ partially mimics the phosphorylated state of RomR, that phosphorylation of D53 is crucial for reversals, and that dynamic RomR localization depends on phosphorylation.

Figure 4 The Frz two-component system regulates RomR localization. Localization of RomR proteins in an *frz* mutant. Cells were transferred from a steady-state culture to an agar pad on a microscope slide and imaged by fluorescence and phase-contrast microscopy. Depicted are overlays of fluorescence and phase-contrast images.

Dynamic RomR localization is regulated by the Frz two-component system

The Frz two-component system regulates the cell reversal frequency, and *frz* mutants only rarely reverse (Blackhart and Zusman, 1985). The correlation between reversals and pole-to-pole transfer of RomR-GFP suggested that the Frz system regulates dynamic RomR localization. To investigate this hypothesis, the gene encoding RomR-GFP was expressed in an *frz, romR::nptII* mutant from the *pilA* promoter (SA2070). In this strain, RomR-GFP localized in a bipolar, asymmetric pattern in all cells, and all cells harbored the large RomR-GFP cluster at the lagging pole (Figure 4; Table I). Single cells of SA2070 did not reverse direction, and RomR-GFP did not relocate between poles (Table I). These data show that the Frz system is dispensable for bipolar, asymmetric RomR localization but required for dynamic RomR localization.

To test whether the Frz system promotes RomR relocation by inducing phosphorylation of RomR, we introduced plasmids encoding $RomR^{D53N}$-GFP and $RomR^{D53E}$-GFP into a *romR*::*nptII* mutant containing the *frz* mutation. $RomR^{D53N}$-GFP (SA2068) localized in a bipolar, asymmetric pattern, with the large RomR cluster at the lagging pole in all cells (Figure 4; Table I). Moreover, as expected, these cells did not reverse direction, and $RomR^{D53N}$-GFP did not relocalize from pole to pole (Table I). $RomR^{D53E}$-GFP (SA2054) localized in a bipolar, asymmetric pattern, with the large RomR cluster at the lagging pole in 71% of cells; in the remaining cells, $RomR^{D53E}$-GFP localized in a bipolar, symmetric pattern (Figure 4; Table I). Importantly, cells containing $RomR^{D53E}$-GFP frequently reversed direction; in cells with an asymmetric pattern, all reversals were accompanied by relocation of $RomR^{D53E}$-GFP, whereas in cells with a symmetric pattern, no relocation was observed (Table I). Thus, $RomR^{D53E}$-GFP, which likely mimics the phosphorylated state of RomR, bypasses the Frz system for reversals. These data suggested that RomR acts downstream of the Frz system to induce reversals in the A-motility system and that the Frz system induces RomR relocation by inducing RomR phosphorylation.

Correct RomR polarity depends on the small GTPase MglA

The MglA protein is important for the activity of both motility systems in *M. xanthus* and has been implicated in the control of the reversal frequency (Spormann and Kaiser, 1999). To

test whether MglA is required for correct RomR localization, we introduced the *romR-gfp* allele into DK3685, which contains the *mglA9* mutation and does not accumulate MglA (Hartzell and Kaiser, 1991a), giving rise to strain SA2042. Strikingly, RomR-GFP localized in a unipolar pattern in 90% of the cells (Figure 5A; Table I). We determined at which pole RomR-GFP localized by staining Tfp with Cy3. Surprisingly, 85% of the cells ($N=32$) contained RomR-GFP and Tfp at the same pole (Figure 5B). Time-lapse microscopy of SA2042 cells was used to monitor the dynamic behavior of RomR-GFP. In these experiments, the cells did not move. This is in contrast to a previous report in which cells with a deletion of *mglA* as well as the upstream *mglB* gene, which codes a protein that stabilizes MglA, were reported to reverse at a high frequency (Spormann and Kaiser, 1999). Under all conditions tested, including those used by Spormann and Kaiser, and also using the Δ*mglBA* strain used by these authors, we were unable to observe movement of *mglA* mutant cells. Notably, RomR-GFP did not undergo pole-to-pole transfer in the *mglA9* mutant. These observations suggested that MglA is required for establishing the correct polarity of the two motility systems and for RomR pole switching.

RomR and FrzS localize independently and relocate synchronously

The two motility systems in *M. xanthus* generate motive force in the same direction (Kaiser and Crosby, 1983; Spormann, 1999) suggesting that the two systems switch polarity in synchrony during cell reversals. The FrzS protein, which is required for the full function of Tfp (Ward *et al*, 2000), localizes in a bipolar, asymmetric pattern, with a large cluster at the leading pole and a small cluster at the lagging pole (Mignot *et al*, 2005). When cells reverse direction, the large FrzS cluster in parallel relocates in an Frz-dependent manner from the old to the new leading pole.

To test whether FrzS is required for correct RomR localization or vice versa, we analyzed RomR-GFP localization in a Δ*frzS* mutant and FrzS-GFP localization in a *romR* mutant. In a Δ*frzS* mutant, RomR-GFP localized in a pattern similar to that in *frzS*$^+$ cells, and all reversals were accompanied by RomR-GFP relocation (SA2268) (Figure 6A; Table I). Likewise, FrzS-GFP localized in the same bipolar, asymmetric pattern in *romR*$^+$ (SA2028) and *romR* (SA2041) cells (Figure 6B). Moreover, 13 out of 15 reversals (25 cells observed) in the *romR*$^+$ strain and 9 out of 10 reversals (25 cells observed) in the *romR* mutant were accompanied by FrzS-GFP relocation from the old to the new leading pole (data not shown). Thus, RomR and FrzS localize to the poles and relocate independently.

To determine whether relocation of RomR and FrzS occurred synchronously, a strain synthesizing FrzS-GFP and RomR fused to monomeric DsRed protein (RomR-mDsRed) (SA2036) was constructed. In a strain containing only RomR-mDsRed, localization was similar to that of RomR-GFP (data not shown). In all SA2036 cells observed ($N=50$), the large FrzS-GFP and RomR-mDsRed clusters localized to opposite poles, with the large FrzS-GFP cluster at the leading and the large RomR-mDsRed cluster at the lagging pole (Figure 6C). In 10 reversals observed (25 cells observed), the large FrzS-GFP and RomR-mDsRed clusters switched poles within 30 s (data for a representative cell are shown in Figure 6C). Thus, FrzS-GFP and RomR-mDsRed oscillate in synchrony.

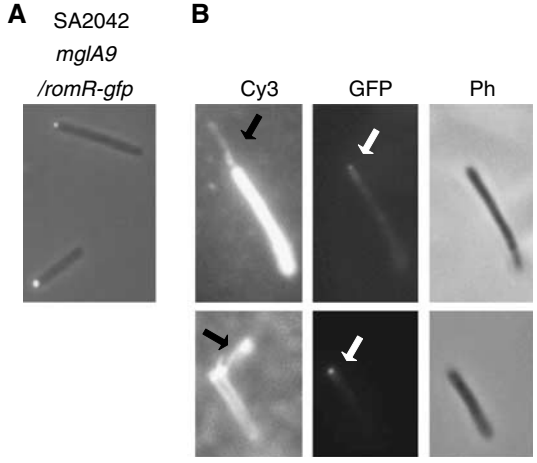

Figure 5 The MglA GTPase regulates RomR localization. (**A**) Localization of RomR-GFP in an *mglA* mutant. Cells from steady-state cultures were transferred to an agar pad on a microscope slide and imaged by fluorescence and phase-contrast microscopy. Depicted are overlays of fluorescence and phase-contrast images. (**B**) The RomR-GFP cluster localizes to the cell pole containing Tfp in the *mglA* mutant. SA2042 cells were harvested from 1% CTT/1.5% agar, stained with Cy3, and inspected by fluorescence microscopy to visualize Tfp (Cy3; black arrows point to Tfp) and RomR-GFP (GFP; white arrows point to large RomR-GFP cluster) and by phase-contrast microscopy (Ph).

Discussion

Localization of proteins to specific subcellular regions is a widely conserved mechanism to spatially confine their activity (Nelson, 2003; Gitai, 2005). Here, we show that the response regulator RomR is required for A-motility in *M. xanthus* and that RomR localizes in a bipolar, asymmetric pattern, with a large cluster at the lagging pole and a smaller cluster at the leading pole. Moreover, RomR localization is dynamic, and RomR relocates between the cell poles in synchrony with cellular reversals. Our data suggest that the large RomR cluster specifies a part of the A-motility machinery located at the lagging cell pole and as such determines in which direction a cell moves, and that dynamic RomR localization is essential for reversals and, thus, for directed, morphogenetic cell movements.

RomR activity depends on bipolar, asymmetric localization

Three lines of evidence suggest that the asymmetric RomR localization pattern is functionally important. First, during a cell reversal, the RomR-GFP clusters initially become equally intense. This change in RomR-GFP distribution is accompanied by an arrest in A-motility-dependent cell movement. Second, after the two RomR-GFP clusters have attained equal intensities, the RomR cluster at the old lagging pole continues to decrease in intensity, whereas the intensity of the cluster at the old leading pole continues to increase. This reversal in RomR polarity is accompanied by the initiation of cell movement in the opposite direction. Third, mutants containing RomR proteins that localize in a bipolar, asymmetric pattern

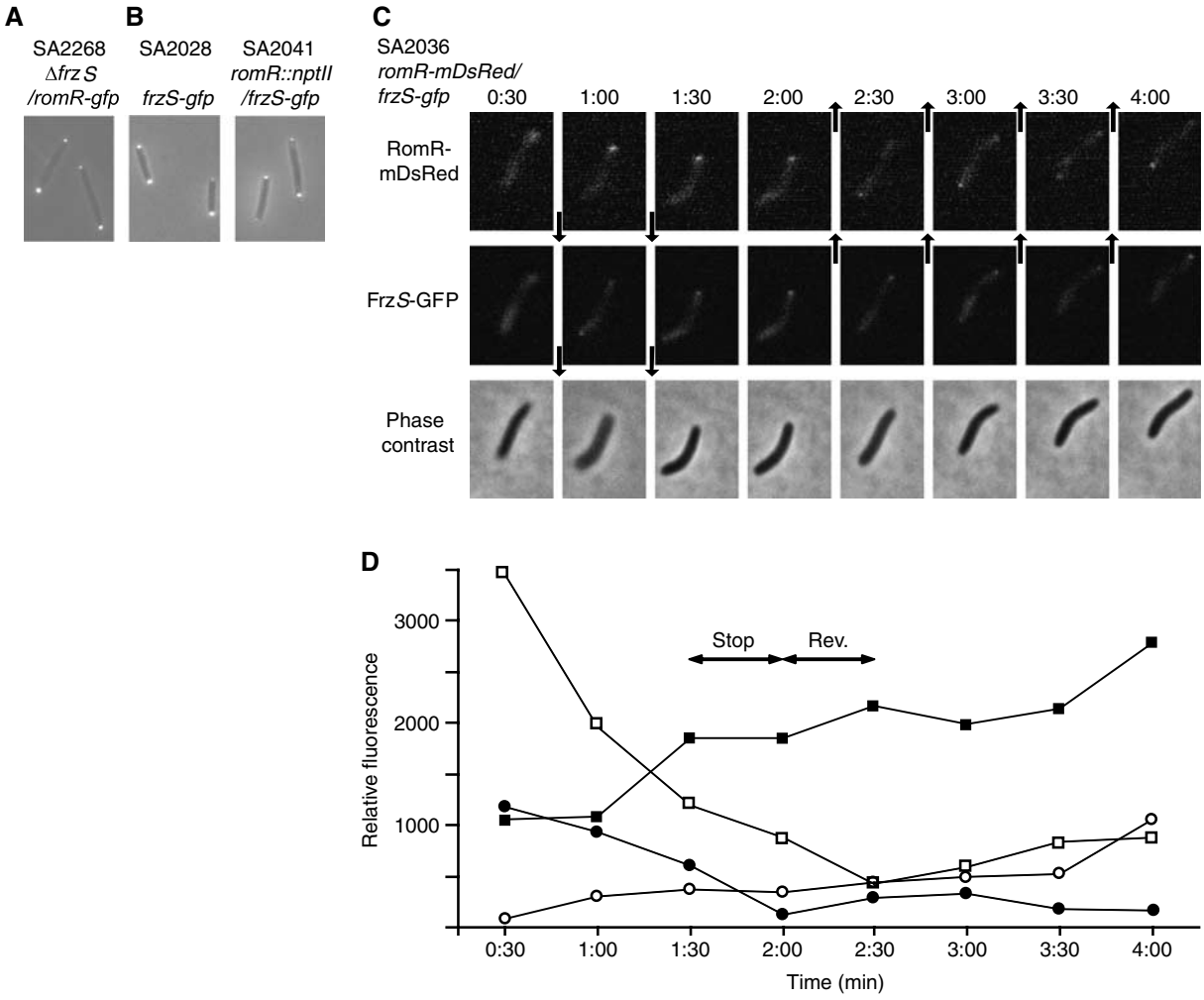

Figure 6 RomR and FrzS localize independently and relocate synchronously. (**A**) RomR-GFP localizes independently of FrzS. Cells were transferred from steady-state cultures to an agar pad on a microscope slide and imaged by fluorescence and phase-contrast microscopy. Depicted are overlays of fluorescence and phase-contrast images. (**B**) FrzS-GFP localizes independently of RomR. Cells were treated and imaged as in (A). Depicted are overlays of fluorescence and phase-contrast images. (**C**) FrzS-GFP and RomR-mDsRed relocate synchronously. Cells were treated as in (A) and imaged by fluorescence and phase-contrast microscopy at 30-s intervals. Shown is a representative cell that underwent one reversal. Depicted are fluorescence images (upper and middle panels) and phase-contrast images (lower panel). Arrows indicate the direction of movement. From 1:30 to 2:00, the cell stopped, and from 2:00 to 2:30, it reversed. (**D**) Quantitative analysis of polar fluorescence signals. The relative fluorescence intensity (arbitrary units) of each pole in the cell in (C) was measured and plotted as a function of time. Squares, FrzS-GFP signals; circles, RomR-mDsRed signals; filled symbols, initial lagging pole; open symbols, initial leading pole. Time intervals with a stop and a reversal (Rev.) are indicated by double-headed arrows.

and are unable to undergo pole-to-pole relocation move unidirectionally, with the large RomR cluster at the lagging pole. According to current models of A-motility, motive force is generated either by multiple AglZ-containing adhesion complexes distributed along the cell body (Mignot *et al*, 2007) or by polyelectrolyte secretion from nozzles at the lagging cell pole (Wolgemuth *et al*, 2002). Our data support a model in which part of the A-motility machinery is located at the lagging pole and in which the large RomR cluster stimulates this machinery. RomR possibly stimulates polyelectrolyte secretion, and the pole-to-pole transfer of the large RomR cluster during a reversal possibly results in inactivation of the nozzles at the old lagging pole and activation of the nozzles at the new lagging pole. We propose that the A-motility machinery is composed of distinct units, with RomR stimulating polyelectrolyte secretion at the lagging pole and AglZ-containing focal adhesion complexes along the cell body. The observations that both *aglZ* and *romR* mutations result in loss of A-motility suggest that the two units are functionally interconnected. We are currently investigating the functional association between these two A-motility units.

Pole-targeting determinants in RomR

Analyses of the localization pattern of mutant RomR proteins consisting of one of the two domains suggested that the output domain is a pole-targeting determinant for RomR and contains the information necessary and sufficient for bipolar, asymmetric localization. These analyses also demonstrated that the receiver domain is dispensable for bipolar, asymmetric localization but indispensable for dynamic RomR localization. Moreover, analyses of other

mutant proteins, specifically RomR^{D53N}, which was unable to relocate between the poles, and RomR^{D53E}, which relocates more frequently between the poles, suggested that residue D53 in the receiver domain of RomR undergoes cycles of phosphorylation and dephosphorylation, with non-phosphorylated RomR being targeted asymmetrically to the poles by the output domain and phosphorylation of D53 triggering the release of RomR. This would then allow RomR to relocate to the opposite pole. Whether RomR is phosphorylated at both poles during the release of RomR or only at the lagging pole remains to be clarified. Although our data suggested that RomR^{D53E} mimics the phosphorylated state of RomR, RomR^{D53E} localizes asymmetrically to the poles. However, polar localization is more transient than that of wild-type RomR, thus giving rise to frequent reversals. We therefore speculate that RomR^{D53E} only partially mimics phosphorylated RomR. Interestingly, in *Caulobacter crescentus*, polar localization of the DivK (Lam *et al*, 2003; Matroule *et al*, 2004) and PleD (Paul *et al*, 2004) response regulators depends on phosphorylation of the conserved Asp residue in the receiver domain. Thus, RomR is distinct from these response regulators in that the localization of non-phosphorylated RomR is polar and phosphorylation causes polar release.

The bipolar, asymmetric localization pattern of RomR points toward the existence of polar, asymmetric targeting factor(s) that interact with the output domain to recruit RomR. The targeting factor(s) either switch from the old lagging pole to the new lagging pole or are unmasked at the new lagging pole and masked at the old lagging pole during a reversal. Proteins involved in A-motility are likely candidates for the polar-targeting factor(s).

The Frz two-component system regulates dynamic RomR localization

RomR pole switching and cell reversals occurred in parallel. From this observation, we infer that RomR does not switch poles because the cells reverse. The Frz two-component system regulates the reversal frequency. In an *frz* mutant, which rarely reverses, RomR-GFP localized in a bipolar, asymmetric pattern without pole switching. Thus, the Frz system is dispensable for bipolar, asymmetric RomR localization. The absence of RomR pole switching in an *frz* mutant, taken together with the inference that RomR does not switch poles because cells reverse, suggested that the Frz system regulates dynamic RomR localization. This hypothesis was confirmed genetically by the observation that the RomR^{D53E} mutant, which likely mimics phosphorylated RomR, bypasses an *frz* mutation, that is, an *frz romR*^{D53E} mutant is able to reverse and RomR^{D53E} is dynamically localized. These data are consistent with the notion that RomR acts downstream of the Frz system to induce reversals in cell direction in the A-motility system and with the Frz system directly or indirectly causing phosphorylation of RomR. The *romR* gene is not flanked by a gene encoding a histidine protein kinase. Thus, the cognate RomR kinase remains unidentified. We are currently testing whether RomR is a direct downstream target of the Frz system, with the FrzE histidine protein kinase phosphorylating RomR, and in this way inducing the release of RomR from the cell pole.

Regulation of the polarity of Tfp and the A-motility system

For the two motility systems in *M. xanthus* to generate motive force in the same direction, they need to switch polarity in synchrony during a reversal. Tfp assembly switches from the old to the new leading pole during a reversal. In parallel, FrzS, which is required for Tfp-dependent motility, and AglZ, which is part of the focal adhesion complexes, relocate from the old to the new leading pole in an Frz-dependent manner (Mignot *et al*, 2005, 2007). These observations suggest that the two motility systems indeed switch polarity synchronously during a reversal. Here, we directly showed that RomR and FrzS localize and relocate between poles independently of each other and that they relocate synchronously. These observations argue against interdependent models for synchronous polarity switching of the two motility systems in which polarity switching of one system drives switching of the other system. Our data rather argue that synchronous polarity switching is brought about by the Frz system inducing the synchronous oscillations of FrzS, RomR, and AglZ.

The Frz-dependent synchronous polarity switching of the two motility systems would maintain the correct polarity of the engines. However, this mechanism does not explain how the correct polarity of the engines is initially established. Interestingly, in a mutant that lacks MglA, a member of the Ras superfamily of small GTPases, RomR localized in a unipolar pattern. Moreover, RomR and Tfp localized to the same pole. These observations suggest that MglA has an essential function in establishing the correct polarity of the two motility systems. In addition, RomR does not relocate between poles in an *mglA* mutant, which suggests that MglA also has a function in regulating dynamic RomR localization. We are currently investigating how MglA interacts with RomR to regulate its localization. In eukaryotic cells, the Ras superfamily of small GTPases controls a wide variety of cellular processes, including cell polarity and cell motility (Etienne-Manneville, 2004). Our findings suggest that the function of small GTPases in establishing cell polarity is not restricted to eukaryotic cells but can be extended to include bacteria.

Bidirectional movement in biological systems

Bidirectional movement of cells and biological structures is a common phenomenon for which several solutions have evolved. Many prokaryotic flagellar motors are switch-like motors that can generate force in both rotational directions (Alam and Oesterhelt, 1984; Blair, 1995). Bidirectional transport along microtubules represents a different solution in which two unidirectional motors, dynein and kinesin, track in opposite directions (Mallik and Gross, 2004). *M. xanthus* illustrates a third strategy for bidirectional movement. *M. xanthus* harbors unidirectional engines, and these engines are combined with mechanisms to regulate their pole-to-pole relocation. With such a mechanism, unidirectional engines are converted into bidirectional engines.

Materials and methods

Growth, motility assays, and development

Construction of strains and plasmids, growth conditions, and motility and development assays are described in Supplementary data. A list of strains used is given in Table II.

Table II *M. xanthus* strains used in this work

Strain	Relevant characteristics[a]	Source or reference
DK1622	Wild type	Kaiser (1979)
DK1217	*aglB1*	Hodgkin and Kaiser (1979)
DK1300	*sglG1*	Hodgkin and Kaiser (1979)
DK1259	*aglB1*, *sglG1*	Hodgkin and Kaiser (1979)
DK6204	Δ*mglAB*	Hartzell and Kaiser (1991b)
DZ4041	*sglA1*, *frzE*::Tn*5*(Tet^r)Ω231	D Zusman
DK10410	Δ*pilA*	Wu and Kaiser (1997)
TM18	Δ*frzS*	T Mignot
DK3685	*mglA9* Tn*5-132* Ω1901	Kroos *et al* (1988)
SA1128	*romR*::*nptII*	This work
SA1131	*romR*::*nptII*, *aglB1*	This work
SA1132	*romR*::*nptII*, *sglG1*	This work
SA2028	*frzS-gfp*	This work
SA2036	*frzS-gfp*, P_{nat}-*romR-mDsRed* (pSL113)	This work
SA2041	*frzS-gfp*, *romR*::*nptII*	This work
SA2042	*mglA9* Tn*5-132* Ω1901/P_{nat}-*romR-gfp* (pSH1208)	This work
SA2054	*frzE*::Tn*5*(Tet^r)Ω231, *romR*::*nptII*/P_{pilA}-*romR*^{D53E}-*gfp* (pGFy166)	This work
SA2058	*romR*::*nptII*/P_{pilA}-*romR-gfp* (pGFy177)	This work
SA2059	*romR*::*nptII*/P_{pilA}-*romR*$^+$ (pGFy175)	This work
SA2060	*romR*::*nptII*/P_{pilA}-*romR*^{D53E}-*gfp* (pGFy166)	This work
SA2061	*romR*::*nptII*/P_{pilA}-*romR*^{D53E} (pGFy165)	This work
SA2062	*romR*::*nptII*/P_{pilA}-*romR*^{D53N}-*gfp* (pGFy178)	This work
SA2063	*romR*::*nptII*/P_{pilA}-*romR*^{D53N} (pGFy176)	This work
SA2068	*frzE*::Tn*5*(Tet^r)Ω231, *romR*::*nptII*/P_{pilA}-*romR*^{D53N}-*gfp* (pGFy178)	This work
SA2070	*frzE*::Tn*5*(Tet^r)Ω231, *romR*::*nptII*/P_{pilA}-*romR-gfp* (pGFy177)	This work
SA2210	*RomR*::*nptII*/pSWU30	This work
SA2244	*romR*::*nptII*/P_{pilA}-*receiver* (pSH1210)	This work
SA2256	*romR*::*nptII*/P_{pilA}-*output* (pSH1211)	This work
SA2259	*romR*::*nptII*/P_{pilA}-*receiver-gfp* (pSH1201)	This work
SA2260	*romR*::*nptII*/P_{pilA}-*output-gfp* (pSH1202)	This work
SA2268	Δ*frzS*/P_{nat}-*romR-gfp* (pSH1208)	This work
SA2271	*romR*::*nptII*/P_{nat}-*romR-gfp* (pSH1208)	This work
SA2272	*romR*::*nptII*/P_{nat}-*romR*$^+$ (pSH1206)	This work
SA2273	P_{nat}-*romR-gfp* (pSH1208)	This work
SA2289	Δ*pilA*, *romR*::*nptII*/P_{nat}-*romR-gfp* (pSH1208)	This work

[a]Plasmids mentioned in parentheses contain the *romR* or *romR-gfp* allele integrated at the chromosomal Mx8 attachment site. Structures of plasmids are shown in Figure 1A. In P_{nat} and P_{pilA} constructs, the *romR* alleles were transcribed from the native *romR* promoter and the *pilA* promoter, respectively.

Microscopy and data analysis

For phase-contrast and fluorescence microscopy, steady-state cultures of *M. xanthus* cells were grown to a density of 7×10^8 cells/ml in liquid CTT medium at 32°C, transferred to a microscope slide with a thin 1.0% agar pad buffered with A50 buffer (10 mM MOPS, pH 7.2, 10 mM $CaCl_2$, 10 mM $MgCl_2$, 50 mM NaCl), and immediately covered with a coverslip. After 30 min at room temperature, cells were observed in a Leica DM6000B microscope, using a Leica Plan Apo × 100/NA 1.40 phase-contrast oil objective, and visualized with a Leica DFC 350FX camera. For fluorescence microscopy, a Leica GFP filter (excitation range 500–550 nm, emission range 450–490 nm) was used for visualizing GFP proteins, and fluorescein-conjugated antibodies and a Y3 filter (excitation range 530–560, emission range 570–650 nm) were used for visualizing RomR-mDsRed- and Cy3-stained cells. Images were recorded and processed with Leica FW4000 V1.2.1 software. Processed images were arranged in Adobe Photoshop 6. For time-lapse recordings, cells were treated as described and imaged at 30-s intervals for 10 min, and images were processed as described. All cells analyzed from the time-lapse recordings were separated from other cells by at least one cell length to ensure that cells moved only by means of the A-motility system. Fluorescence signals were quantified using the region measurement tool in Metamorph 7.0r2 (Visitron Systems). Immunofluorescence microscopy was as described (Mignot *et al*, 2005). Briefly, *M. xanthus* cells were grown as described and fixed with 2.6% paraformaldehyde and 0.008% glutaraldehyde for 20 min on freshly prepared poly-L-lysine-treated 12-well diagnostic slides (Erie Scientific Company). Cells were permeabilized with 0.2 μg/ml lysozyme for 4 min and probed with affinity-purified, rabbit polyclonal anti-RomR antibodies at 4°C overnight in PBS buffer (137 mM NaCl, 2.7 mM KCl, 10 mM Na_2HPO_4, 1.8 mM KH_2PO_4, pH 7.4) supplemented with 2% BSA. Fluorescein-conjugated goat anti-rabbit antibodies (Perbio Science) were used as a secondary antibody. Slow Fade Anti Fade Reagent (Molecular Probes) was added to each well, and cells were visualized and imaged as described. To stain Tfp, the procedure of Skerker and Berg (2001) was adapted. Briefly, cells were grown on 1.5% agar plates supplemented with 1% CTT, scraped off the agar, and resuspended in 100 μl labeling buffer (50 mM KPO_4, pH 8.0, 5 mM $MgCl_2$, 25 μM EDTA). Cells were harvested by gentle centrifugation and gently resuspended in labeling buffer. This step was repeated three times. Cy3 from one vial (Amersham Biosciences) was dissolved in 250 μl labeling buffer and added to the cells, and the mixture was incubated for 1 h at 20°C. Cells were washed three times in labeling buffer, spotted onto a glass slide, covered with a coverslip, and visualized as described above.

Purification of RomR and immunoblot analysis

Purification of RomR for generating anti-RomR antibodies and immunoblotting is described in Supplementary data.

Supplementary data

Supplementary data are available at *The EMBO Journal* Online (http://www.embojournal.org).

Acknowledgements

We thank T Mignot and D Zusman for providing strains and plasmids, R Müller for access to the *Sorangium cellulosum* genome sequence, and Steffi Lindow for excellent technical assistance. The graduate program 'Intra- and intercellular transport and communication' and the Max Planck Society supported this work.

References

Alam M, Oesterhelt D (1984) Morphology, function and isolation of halobacterial flagella. *J Mol Biol* **176:** 459–475

Blackhart BD, Zusman DR (1985) 'Frizzy' genes of *Myxococcus xanthus* are involved in control of frequency of reversal of gliding motility. *Proc Natl Acad Sci USA* **82:** 8771–8774

Blair DF (1995) How bacteria sense and swim. *Annu Rev Microbiol* **49:** 489–522

Domian IJ, Quon KC, Shapiro L (1997) Cell type-specific phosphorylation and proteolysis of a transcriptional regulator controls the G1-to-S transition in a bacterial cell cycle. *Cell* **90:** 415–424

Etienne-Manneville S (2004) Cdc42—the centre of polarity. *J Cell Sci* **117:** 1291–1300

Gitai Z (2005) The new bacterial cell biology: moving parts and subcellular architecture. *Cell* **120:** 577–586

Hartzell P, Kaiser D (1991a) Function of MglA, a 22-kilodalton protein essential for gliding in *Myxococcus xanthus*. *J Bacteriol* **173:** 7615–7624

Hartzell P, Kaiser D (1991b) Upstream gene of the *mgl* operon controls the level of MglA protein in *Myxococcus xanthus*. *J Bacteriol* **173:** 7625–7635

Hartzell PL (1997) Complementation of sporulation and motility defects in a prokaryote by a eukaryotic GTPase. *Proc Natl Acad Sci USA* **94:** 9881–9886

Hodgkin J, Kaiser D (1979) Genetics of gliding motility in *Myxococcus xanthus* (Myxobacterales): two gene systems control movement. *Mol Gen Genet* **171:** 177–191

Hoiczyk E, Baumeister W (1998) The junctional pore complex, a prokaryotic secretion organelle, is the molecular motor underlying gliding motility in cyanobacteria. *Curr Biol* **8:** 1161–1168

Kaiser D (1979) Social gliding is correlated with the presence of pili in *Myxococcus xanthus*. *Proc Natl Acad Sci USA* **76:** 5952–5956

Kaiser D, Crosby C (1983) Cell movements and its coordination in swarms of *Myxococcus xanthus*. *Cell Motility* **3:** 227–245

Kroos L, Hartzell P, Stephens K, Kaiser D (1988) A link between cell movement and gene expression argues that motility is required for cell–cell signaling during fruiting body development. *Genes Dev* **2:** 1677–1685

Lam H, Matroule JY, Jacobs-Wagner C (2003) The asymmetric spatial distribution of bacterial signal transduction proteins coordinates cell cycle events. *Dev Cell* **5:** 149–159

Mallik R, Gross SP (2004) Molecular motors: strategies to get along. *Curr Biol* **14:** R971–R982

Matroule JY, Lam H, Burnette DT, Jacobs-Wagner C (2004) Cytokinesis monitoring during development: rapid pole-to-pole shuttling of a signaling protein by localized kinase and phosphatase in *Caulobacter*. *Cell* **118:** 579–590

Mattick JS (2002) Type IV pili and twitching motility. *Annu Rev Microbiol* **56:** 289–314

Merz AJ, So M, Sheetz MP (2000) Pilus retraction powers bacterial twitching motility. *Nature* **407:** 98–102

Mignot T, Merlie JP, Zusman DR (2005) Regulated pole-to-pole oscillations of a bacterial gliding motility protein. *Science* **310:** 855–857

Mignot T, Shaevitz JW, Hartzell PL, Zusman DR (2007) Evidence that focal adhesion complexes power bacterial gliding motility. *Science* **315:** 853–856

Nelson WJ (2003) Adaptation of core mechanisms to generate cell polarity. *Nature* **422:** 766–774

Paul R, Weiser S, Amiot NC, Chan C, Schirmer T, Giese B, Jenal U (2004) Cell cycle-dependent dynamic localization of a bacterial response regulator with a novel di-guanylate cyclase output domain. *Genes Dev* **18:** 715–727

Shi W, Zusman DR (1993) The two motility systems of *Myxococcus xanthus* show different selective advantages on various surfaces. *Proc Natl Acad Sci USA* **90:** 3378–3382

Skerker JM, Berg HC (2001) Direct observation of extension and retraction of type IV pili. *Proc Natl Acad Sci USA* **98:** 6901–6904

Søgaard-Andersen L (2004) Cell polarity, intercellular signalling and morphogenetic cell movements in *Myxococcus xanthus*. *Curr Opin Microbiol* **7:** 587–593

Spormann AM (1999) Gliding motility in bacteria: insights from studies of *Myxococcus xanthus*. *Microbial Mol Biol Rev* **63:** 621–641

Spormann AM, Kaiser D (1999) Gliding mutants of *Myxococcus xanthus* with high reversal frequencies and small displacements. *J Bacteriol* **181:** 2593–2601

Stock AM, Robinson VL, Goudreau PN (2000) Two-component signal transduction. *Annu Rev Biochem* **69:** 183–215

Sun H, Zusman DR, Shi W (2000) Type IV pilus of *Myxococcus xanthus* is a motility apparatus controlled by the *frz* chemosensory system. *Curr Biol* **10:** 1143–1146

Ward MJ, Lew H, Zusman DR (2000) Social motility in *Myxococcus xanthus* requires FrzS, a protein with an extensive coiled-coil domain. *Mol Microbiol* **37:** 1357–1371

Wolgemuth C, Hoiczyk E, Kaiser D, Oster G (2002) How myxobacteria glide. *Curr Biol* **12:** 369–377

Wu SS, Kaiser D (1997) Regulation of expression of the *pilA* gene in *Myxococcus xanthus*. *J Bacteriol* **179:** 7748–7758

Youderian P, Burke N, White D, Hartzell PL (2003) Identification of genes required for adventurous gliding motility in *Myxococcus xanthus* with the transposable element *mariner*. *Mol Microbiol* **49:** 555–570

Yu R, Kaiser D (2007) Gliding motility and polarized slime secretion. *Mol Microbiol* **63:** 454–467

